Inorganic Chemistry
Article
Cite This: Inorg. Chem. XXXX, XXX, XXX−XXX
pubs.acs.org/IC

Oxygen Atom Transfer to Cationic PCPNi(II) Complexes Using Amine-*N*-Oxides

Etienne A. LaPierre,[†] Marissa L. Clapson,[†] Warren E. Piers,*[,†] Laurent Maron,*[,‡] Denis M. Spasyuk,[§] and Chris Gendy[†]

[†]Department of Chemistry, University of Calgary, 2500 University Drive N.W., Calgary, Alberta, Canada T2N 1N4
[‡]LPCNO, Université de Toulouse, INSA, UPS, LPCNO, 135 avenue de Rangueil, F-31077 Toulouse, France
[§]Canadian Light Source, Inc., 44 Innovation Boulevard, Saskatoon, Saskatchewan, Canada S7N 2V3

Supporting Information

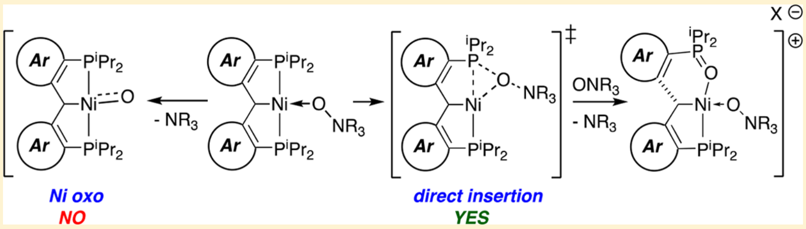

ABSTRACT: Three $PC_{sp3}P$ pincer ligands differing in the aryl group linking the phosphine arms with the anchoring carbon donor were used to support square planar Ni(II) bromide complexes $\mathbf{1}$−$\mathbf{3}_{Br}$. Exchange of the coordinating bromide anion for the more weakly coordinating triflate (OTf) or hexafluoroantimonate (SbF_6) anions was accomplished by treatment with AgX or TlX salts to give compounds $\mathbf{1}$−$\mathbf{3}_X$; compounds $\mathbf{1}_{OTf}$, $\mathbf{1}_{SbF_6}$, $\mathbf{2}_{Br}$, $\mathbf{2}_{OTf}$, $\mathbf{3}_{Br}$, and $\mathbf{3}_{SbF_6}$ were all characterized by X-ray crystallography. The reactions of these Ni(II) compounds with the amine-*N*-oxide oxygen atom transfer agents $ONMe_3$ and $ONMePh_2$ were explored. For $ONMe_3$, reactions with 2 equiv gave products in which one arm of the pincer ligand was oxidized to a P═O unit, with the other amine-*N*-oxide ligated to the Ni(II) center, forming products $\mathbf{5}$−$\mathbf{6}_X$; compounds $\mathbf{4}_{OTf}$, $\mathbf{5}_{OTf}$, and $\mathbf{6}_{SbF_6}$ were characterized crystallographically. Transient amine-*N*-oxide adducts prior to ligand oxidation were observed in some reactions. For the more effective O atom donor $ONMePh_2$, reactions were very rapid and a second oxidation of the remaining phosphine arm was observed, producing a Ni(II) species with an OCO pincer ligand ($\mathbf{7}_{SbF_6}$). All compounds were fully characterized. Experiments aimed at trapping transient Ni(IV) oxo intermediates (with cyclohexadiene, KH, and various Lewis acids) indicated that such species were not involved in the reaction. This was supported by density functional theory (DFT) computations at the B3PW91 level, which indicated that direct O atom insertion into the Ni−P bonds without the intermediacy of a Ni oxo species was the low-energy pathway.

■ INTRODUCTION

Late-transition-metal terminal oxo complexes represent a challenging and intriguing target for synthetic inorganic and organometallic chemists. These complexes are proposed as intermediates in a variety of catalytic and biomimetic reactions, such as oxidation of hydrocarbons[1−7] and water splitting schemes.[8−16] However, late-transition-metal oxo complexes (as well as related nitride complexes) are fundamentally unstable, because of the population of M−E (E = N, O) π^*-orbitals.[17−20] Because of this destabilizing bonding situation, examples of transition-metal multiple bonds in complexes with a tetragonal ligand field past group 8 are sparse, since the high oxidation states required for necessarily low enough *d*-electron counts are less accessible.

The degree of π^*-orbital population is dependent on molecular symmetry and *d*-electron count, with square planar complexes tolerating higher *d*-electron counts than octahedral complexes.[18,21,22] Thus, one strategy for the stabilization of later-metal-element multiple bonds is through the use of tridentate pincer ligands, which provide a rigid, chelating ligand array that enforces a square planar geometry. While this strategy has met with modest success, leading to the isolation and structural characterization of iridium nitrido complexes,[22,23] and the isolation of a compound proposed to be a platinum-oxo complex,[24] for the most part, intermediary or transiently generated oxo and nitrido complexes have eluded explicit structural elucidation.[25−33] Spectroscopic observation has been noted in some cases,[25−27,30,34−36] but evidence for these species often hinges on the characterization of the products of trapping experiments with external reagents or isolation of "decomposition" products[28,29,31,32] resulting from the oxidation of one or both of the arms (usually phosphines) of the pincer ligand framework. Products arising from E-centered radical chemistry

Received: October 29, 2017

DOI: 10.1021/acs.inorgchem.7b02766
Inorg. Chem. XXXX, XXX, XXX−XXX

have also been observed, such as radical coupling of nitride ligands[22,27] or H atom abstraction.[28,32] Perhaps the most notable example of the former is the slow conversion of Milstein's aforementioned platinum-oxo complex (which, to date, is the only claimed example of an isolated terminal group 10 metal multiple bond in a tetragonal ligand field) to the PCO pincer complex in which the oxo has been inserted into the Pt−P bond (Scheme 1a).[24] In other systems, such as the PNPNi(IV) nitrido complex proposed by van der Vlugt and co-workers (Scheme 1b), the ligand oxidation is too rapid for observation of the transient Ni nitride; the resulting product of nitrido insertion rapidly activates the C−H bond of benzene.[29] This contrasts with a variety of group 9 systems where the primary decomposition pathway is ligand C−H bond activation,[28,32,34] or radical coupling of nitride ligands to yield dinitrogen adducts.[22,27] However, there are cobalt-based systems in which ligand oxidation is the primary mode of reactivity, such as Meyer's tripodal Co(IV) nitride complex,[30] and complexes arising from oxygen atom transfer to Caulton's PNPCo(I) complex (Scheme 1c).[26]

Scheme 1

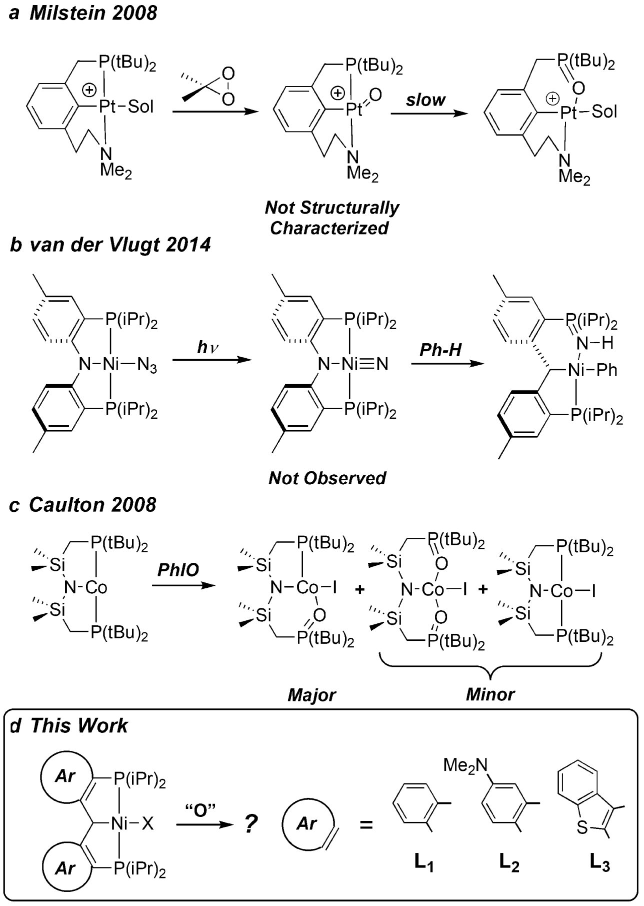

Attempted generation of a high-valency nickel-oxo species via oxygen transfer reactions is of particular interest, given the relative dearth of examples of tetragonal group 10 metal compounds with multiple bonds, the reported evidence for isolation of a Pt(IV) oxo complex,[24] and the potential importance of these species in Ni-catalyzed oxidation reactions.[36] We recently developed a rigid PCP pincer ligand modeled after the PNP ligand system featured in the van der Vlugt chemistry of Scheme 1b. The PCP system is somewhat more electron-donating,[37,38] in comparison, and the anchoring carbon donor can be sp^3 or sp^2 hybridized, creating the possibility of ligand cooperativity.[39] Furthermore, modifications to the aryl group linking the ligand arms to the central donor can provide another lever for electron-donating control.[40] Nickel(II) complexes of these ligands can be readily prepared,[41−43] and herein we explore the reactivity of three such complexes (Scheme 1d) with oxygen atom transfer agents. The parent phenyl linked system L_1 can be made more electron-donating via incorporation of an NMe_2 group *para* to the central carbon donor, (L_2) while the benzothiophene linked ligand, L_3,[44] is a more planar, rigidified structure. With this array of ligands, the potential intermediacy of a high-valency nickel-oxo complex was explored; however, in each system, oxygen atom insertion into the Ni−P bonds of the ligand was observed, with no experimental or computational evidence for Ni oxo species on the reaction path. The implications of these observations for further ligand design are discussed.

■ EXPERIMENTAL SECTION

For general experimental considerations and modified syntheses of starting materials $\mathbf{L_1}$ and $\mathbf{1_{Br}}$,[41] see the Supporting Information.

Synthesis of Diphenylmethylamine-*N*-oxide ($ONPh_2Me$). To a 150-mL round-bottom flask was added 1.073 g of methyldiphenylamine (6.22 mmol) dissolved in ca. 75 mL of chloroform. In a second 150 mL round-bottom flask, 2.015 g of 72% *m*-chloroperbenzoic acid (11.0 mmol, 1.25 equiv) was dissolved in 50 mL of chloroform. The solution of methyldiphenylamine was cooled in an ice bath and the solution of *m*-chloroperbenzoic acid was added dropwise to the solution of the amine over 10 min. The solution was warmed to room temperature and stirred for 18 h. A color change from clear to light orange was observed. Solvent was removed in vacuo and the crude mixture purified by column chromatography on 60 g of basic alumina using 3:1 $CHCl_3$:CH_3OH as an eluent. Fractions containing product ($R_f = 0.9$) were combined and solvent removed in vacuo. The residue was dissolved in minimal hot acetone, layered with hexanes and cooled to −20 °C for 72 h to yield a beige powder (0.838 g, 4.21 mmol, 72% yield). ^{1}H NMR (500 MHz, Chloroform-d) δ 7.73 (dd, J = 7.9, 1.8 Hz, 4H, Ar-H), 7.40 (m, 4H. Ar-H), 7.37−7.31 (m, 2H, Ar-H), 3.93 (s, 3H, CH_3). ^{13}C NMR (126 MHz, methylene chloride-d_2) δ 129.15, 128.64, 121.43, 62.53. HRMS (ESI) Calcd: 200.107, Found: 200.1076.

Synthesis of $\mathbf{1_{OTf}}$. To a solution of $\mathbf{1_{Br}}$ (300 mg, 0.557 mmol) in THF (3 mL) was added 1.05 equiv of AgOTf (150 mg, 0.583 mmol), resulting in the immediate precipitation of AgBr. The suspension was filtered through a 0.1 μm PTFE syringe filter and the filtrate is concentrated under reduced pressure to yield a red solid. The solid was extracted into minimal toluene (~2 mL) and resulting solution was layered with ~15 mL of *n*-pentane and refrigerated at −30 °C overnight to yield red-orange block crystals of $\mathbf{1_{OTf}}$. Yield: 277 mg (0.457 mmol, 82%). ^{31}P NMR (243 MHz, benzene-d_6) δ 44.1. ^{1}H NMR (600 MHz, benzene-d_6) δ 7.07−7.02 (m, 2H, Ar-H), 6.97−6.90 (m, 4H, Ar-H), 6.87 (t, J = 7.2 Hz, 2H, Ar-H), 5.35 (s, 1H, Ni−CH), 2.67 (ddq, J = 14.3, 7.1, 4.4, 2.6 Hz, 2H, CH_3−CH−CH_3), 2.21 (ddq, J = 10.5, 7.1, 3.2 Hz, 2H, CH_3−CH−CH_3), 1.45 (dd, J = 8.9, 7.1 Hz, 6H, CH−(CH_3)$_2$), 1.38 (dd, J = 7.7 Hz, 6H, CH−(CH_3)$_2$), 1.13 (dd, J = 7.6 Hz, 6H CH−(CH_3)$_2$), 1.00 (dd, J = 6.6 Hz, 6H, CH−(CH_3)$_2$). ^{13}C NMR (126 MHz, benzene-d_6) δ 157.30 (t, J = 17.2 Hz, P-C_{aryl}), 130.96, 130.71 (t, J = 19.5 Hz, C_{aryl}), 129.50(C_{aryl}), 125.52 (t, J = 6.7 Hz, C_{aryl}), 124.65 (t, J = 3.2 Hz, C_{aryl}), 34.69 (t, J = 7.8 Hz, Ni-C), 23.75 (t, J = 10.8 Hz, CH−(CH_3)$_2$), 23.15 (t, J = 9.2 Hz, CH−(CH_3)$_2$), 19.02 (t, J = 3.2 Hz, CH−(CH_3)$_2$), 18.08 (CH−(CH_3)$_2$), 17.26 (CH−(CH_3)$_2$), 16.18 (CH−(CH_3)$_2$). ^{19}F NMR (471 MHz, benzene-d_6) δ −78.2. Elemental Analysis: Calcd (%): C 51.42; H 6.14. Found: C 51.50; H 6.11.

Synthesis of $\mathbf{1_{SbF_6}}$. To a solution of $\mathbf{1_{Br}}$ (500 mg, 0.929 mmol) in THF (3 mL) was added 1.00 equiv of $AgSbF_6$ (320 mg, 0.929 mmol), resulting in the immediate precipitation of AgBr. The suspension was filtered through a 0.1 μm polytetrafluoroethylene (PTFE) syringe filter and the filtrate was concentrated under reduced pressure and the residue was extracted into minimal DCM, layered with 15 mL of *n*-pentane and refrigerated at −30 °C for 3 days to yield a red microcrystalline solid. Crystals suitable for analysis by single-crystal X-ray diffraction (XRD) studies were grown by layering 1 mL of a 50 mg/mL DCM solution of $\mathbf{1}_{\mathbf{SbF_6}}$ with 3 mL of *n*-pentane and refrigerating at −30 °C for 3 days, yielding orange plates. Yield: 627 mg (0.818 mmol, 88%). ^{31}P NMR (243 MHz, methylene chloride-d_2) δ 43.1. ^{1}H NMR (600 MHz, methylene chloride-d_2) δ 7.47 (dq, J = 7.4, 3.6 Hz, 2H, Ar-**H**), 7.35−7.28 (m, 4H, Ar-**H**), 7.09 (dd, J = 6.2, 3.2 Hz, 2H, Ar-**H**), 5.55−5.44 (m, 1H, Ni−C**H**), 3.84 (s, 4H, THF O−C**H**$_2$), 2.58−2.49 (m, 2H, C**H**−(CH$_3$)$_2$), 2.42 (s, 2H, C**H**−(CH$_3$)$_2$), 1.96 (s, 4H, THF O−CH$_2$−C**H**$_2$), 1.46 (dd, J = 8.0 Hz, 6H, CH−(C**H**$_3$)$_2$), 1.42−1.36 (m, 6H, CH−(C**H**$_3$)$_2$), 1.39−1.26 (m, 12H, CH−(C**H**$_3$)$_2$). ^{13}C NMR (151 MHz, CD$_2$Cl$_2$) δ 156.4 (P-C_{aryl}), 131.65 (C_{aryl}), 131.08 (C_{aryl}), 128.92 (C_{aryl}), 126.35 (C_{aryl}), 126.17 (C_{aryl}), 25.15 (CH−(CH$_3$)$_2$), 24.66 (CH−(CH$_3$)$_2$), 19.15 (CH−(CH$_3$)$_2$), 18.70 (CH−(CH$_3$)$_2$), 18.43 (CH−(CH$_3$)$_2$), 17.52 (CH−(CH$_3$)$_2$). All peaks in the spectra are characteristically broad; the carbon bound to nickel and the THF carbons are not observed. Elemental analysis: Calcd (%): C 45.47; H 5.92. Found: C 42.94; H 6.09. (Carbon content low due to the presence of DCM in the crystal lattice.)

Synthesis of $\mathbf{2}_{\mathbf{Br}}$. To a solid mixture of 475 mg of $\mathbf{L_2}$ (0.976 mmol) and 300 mg of NiBr$_2$(MeCN)$_2$ (0.976 mmol) in a 50-mL thick-walled glass vessel with a Kontes needle valve was added 25 mL of tetrahydrofuran (THF) and 1 mL of NEt$_3$. The vessel was sealed and heated to 65 °C for 18 h to yield a dark brown solution. The solvent was removed in vacuo and the residue was extracted into toluene and filtered to remove triethylammonium bromide. The filtrate was concentrated, dissolved in 50 mL of Et$_2$O, and filtered, leaving behind a blue residue, which was discarded. The filtrate was concentrated and the residue was recrystallized by layering a concentrated toluene solution (~2 mL) with 15 mL of *n*-pentane and cooling to −30 °C for 2 days, yielding orange-red plate crystals of $\mathbf{2}_{\mathbf{Br}}$. Yield: 301 mg (49%, 0.478 mmol). ^{31}P NMR (243 MHz, benzene-d_6) δ 45.4 ^{1}H NMR (600 MHz, benzene-d_6) δ 7.38 (dd, J = 8.5, 1.3 Hz, 2H, Ar-*H*), 6.76 (q, J = 3.5 Hz, 2H, Ar-*H*), 6.59 (dd, J = 8.6, 2.6 Hz, 2H, Ar-*H*), 5.53 (s, 1H, Ni-*H*), 2.71−2.64 (m, 2H, C*H*(CH$_3$)$_2$), 2.63−2.55 (m, 2H C*H*(CH$_3$)$_2$), 2.54 (s, 12H, N-(C*H*$_3$)), 1.63 (dd, J = 7.3 Hz, 6H, CH(C*H*$_3$)$_2$), 1.55 (dd, J = 7.6 Hz, 6H, CH(C*H*$_3$)$_2$), 1.34 (dd, J = 7.2 Hz, 6H, CH(C*H*$_3$)$_2$), 1.28 (dd, J = 6.8 Hz, 6H, CH(C*H*$_3$)$_2$). ^{13}C NMR (151 MHz, benzene-d_6) δ 148.19 (t, J = 3.3 Hz, NMe$_2$-H_{aryl}), 147.91 (t, J = 18.1 Hz, P-H_{aryl}), 135.01 (t, J = 17.4 Hz, H_{aryl}), 126.61 (t, J = 8.1 Hz, H_{aryl}), 115.14 (C_{aryl}), 114.37 (C_{aryl}), 44.48 (t, J = 7.9 Hz, Ni−C*H*), 40.24 (N-CH$_3$), 25.19 (t, J = 11.4 Hz, CH(CH$_3$)$_2$), 24.75 (t, J = 9.6 Hz, CH(CH$_3$)$_2$), 19.28 (t, J = 2.6 Hz, CH(CH$_3$)$_2$), 18.77 (CH(CH$_3$)$_2$), 18.47 (CH(CH$_3$)$_2$), 17.87 (CH(CH$_3$)$_2$). Elemental analysis: Calcd (%): C 55.80; H 7.59; N 4.49. Found: C 56.18; H 7.66; N 4.26.

Synthesis of $\mathbf{2}_{\mathbf{OTf}}$. To a solution of $\mathbf{2}_{\mathbf{Br}}$ (100 mg, 0.160 mmol) in DCM (3 mL) was added 1.05 equiv of TlOTf (60 mg, 0.168 mmol), resulting in the immediate precipitation of TlBr. The suspension was filtered through a 0.1 μm PTFE syringe filter and the filtrate was concentrated under reduced pressure to yield a red solid. The solid was extracted into minimal toluene (~2 mL), and the resulting solution was layered with ~15 mL of *n*-pentane and refrigerated at −30 °C overnight to yield an off-white residue. The mother liquor was decanted and cooled to −30 °C overnight to yield orange block crystals of the $\mathbf{2}_{\mathbf{OTf}}$. Yield: 68 mg (61%, 0.098). ^{31}P NMR (203 MHz, benzene-d_6) δ 43.2. ^{1}H NMR (500 MHz, benzene-d_6) δ 7.12−7.07 (m, 2H, Ar-*H*), 6.62 (dd, J = 3.6 Hz, 2H, Ar-*H*), 6.44 (dd, J = 8.7, 2.6 Hz, 2H, Ar-*H*), 5.40 (s, 1H, Ni−C*H*), 2.74 (tt, J = 7.1, 2.6 Hz, 2H, C*H*(CH$_3$)$_2$), 2.46 (s, 12H), 2.32 (td, J = 7.3, 3.5 Hz, 2H, C*H*(CH$_3$)$_2$), 1.54 (dd, J = 8.9, 7.2 Hz, 6H, CH(C*H*$_3$)$_2$), 1.46 (dd, J = 7.5 Hz, 6H, CH(C*H*$_3$)$_2$), 1.27 (dd, J = 7.4 Hz, 6H, CH(C*H*$_3$)$_2$), 1.11 (dd, J = 6.5 Hz, 6H, CH(C*H*$_3$)$_2$). ^{13}C NMR (126 MHz, benzene-d_6) δ 147.77 (t, J = 3.5 Hz, NMe$_2$-C_{aryl}), 145.99 (t, J = 17.1 Hz, P-C_{aryl}), 131.31 (t, J = 19.1 Hz, C_{aryl}), 125.77 (t, J = 7.9 Hz, C_{aryl}), 114.47 (C_{aryl}), 113.61 (C_{aryl}), 39.40 (N-(CH$_3$)$_2$), 33.51 (t, J = 6.5 Hz, Ni-CH), 23.83 (t, J = 10.4 Hz, CH(CH$_3$)$_2$), 23.30 (t, J = 8.9 Hz, CH(CH$_3$)$_2$), 19.15 (t, J = 3.3 Hz, CH(CH$_3$)$_2$), 18.28 (CH(CH$_3$)$_2$), 17.49 (d, J = 2.4 Hz, CH(CH$_3$)$_2$), 16.57 (CH(CH$_3$)$_2$). ^{19}F NMR (471 MHz, benzene-d_6) δ −78.2. Elemental analysis: Calcd (%): C 51.96; H 6.83; N 4.04. Found: C 52.10; H 6.64; N 3.99.

Synthesis of $\mathbf{3}_{\mathbf{Br}}$. To a 25-mL thick-walled glass vessel equipped with a Kontes needle valve was added $\mathbf{L_3}$ (315 mg, 0.614 mmol), NiBr$_2$(MeCN)$_2$ (188 mg, 0.625 mmol), and NEt$_3$ (0.24 mL). The solids were dissolved in ca. 4 mL of bromobenzene and the solution was heated for 18 h at 60 °C. The reaction solution was cooled and filtered through a 0.1 μm PTFE syringe filter into a 50 mL round-bottom flask. The flask was rinsed with ca. 2 mL of toluene and filtered. Solvents were removed in vacuo, and the residue was triturated with pentane. Solvents were again removed in vacuo to yield a red-brown solid. Crystals suitable for analysis by single-crystal XRD studies were grown by vapor diffusion using minimal toluene and pentane and cooling the system at −30 °C for 24 h. Yield: 392 mg (0.603 mmol, 98%). ^{31}P NMR (162 MHz, benzene-d_6) δ 40.7. ^{1}H NMR (400 MHz, benzene-d_6) δ 7.60 (d, $^{3}J_{HH}$ = 8.1 Hz, 2H, Ar-*H*), 7.49 (d, $^{3}J_{HH}$ = 8.1 Hz, 2H, Ar-*H*), 7.01 (t, $^{3}J_{HH}$ = 7.5 Hz, 2H. Ar-*H*), 5.40 (s, 1H, Ni−C*H*), 1.57 (dq, $^{2}J_{HP}$ = 15.8, $^{3}J_{HH}$ = 7.8 Hz, 4H, C*H*(CH$_3$)$_2$), 1.29 (q, $^{3}J_{HP}$ = $^{3}J_{HH}$ = 7.8 Hz, 12H, CH(C*H*$_3$)$_2$), 1.16 (q, $^{3}J_{HP}$ = $^{3}J_{HH}$ = 7.2 Hz, 12H, CH(C*H*$_3$)$_2$). ^{13}C NMR (126 MHz, benzene-d_6) δ 169.58 (vt, J_{PC} = 26.3, 25.7 Hz, Ar-*C*-P), 144.71 (vt, J_{PC} = 3.4 Hz, Ar-*C*), 136.70 (s, Ar-*C*), 128.37 (s, Ar-*C*), 124.73 (s, Ar-*C*), 123.91 (s, Ar-*C*), 122.95 (s, Ar-*C*)), 122.22 (s, Ar-*C*), 34.18 (s, Ni-CH), 24.74 (t, J = 10.8 Hz, *C*(CH$_3$)$_2$), 24.14 (t, J = 12.5 Hz, *C*(CH$_3$)$_2$), 18.98 (s, CH(*C*H$_3$)$_2$), 18.72 (s, CH(*C*H$_3$)$_2$), 18.62 (s, CH(*C*H$_3$)$_2$), 18.31 (s, CH(*C*H$_3$)$_2$). Elemental analysis: Calcd (%): C, 53.48; H, 5.88. Found: C, 54.03; H, 5.74.

Synthesis of $\mathbf{3}_{\mathbf{SbF_6}}$. In a 1 dram vial, $\mathbf{3}_{\mathbf{Br}}$ (279 mg, 0.318 mmol) and AgSbF$_6$ (147 mg, 428 mmol) were dissolved in 1.5 mL of THF. The reaction mixture was agitated for 1 min and allowed to sit at room temperature for 1 h, resulting in the formation of a white precipitate. The reaction mixture was filtered through a 0.1 μm PTFE syringe filter into a 50 mL round-bottom flask. Solvent was removed in vacuo, and the resulting crude solid triturated with ca. 2 mL of pentane. The final product was dried in vacuo to yield a dark purple powder. Crystals suitable for analysis by single-crystal XRD studies were grown by dissolving a 15 mg portion of the final product in minimal dichloromethane, layered with hexanes in a small vial, and placing in the freezer at −30 °C. Red crystals were collected after 2 days. Yield: 194 mg (0.221 mmol, 69%). ^{31}P{^{1}H} NMR (203 MHz, methylene chloride-d_2) δ 37.2. ^{1}H NMR (500 MHz, methylene chloride-d_2) δ 7.82 (d, $^{3}J_{HH}$ = 7.9 Hz, 2H, Ar-*H*), 7.78 (d, $^{3}J_{HH}$ = 8.0 Hz, 2H, Ar-*H*), 7.44−7.33 (m, 4H, Ar-*H*), 5.59 (s, 1H, Ni−C*H*), 2.80 (s, 4H, C*H*(CH$_3$)$_2$), 1.69−1.60 (m, 6H, CH(C*H*$_3$)$_2$), 1.60−1.50 (m, 6H, CH(C*H*$_3$)$_2$), 1.43 (p, $^{3}J_{HP}$ = $^{3}J_{HH}$ = 7.0 Hz, 12H, CH(C*H*$_3$)$_2$). ^{13}C NMR (126 MHz, methylene chloride-d_2) δ 168.24 (s, Ar-*C*), 144.68 (s, Ar-*C*), 137.47 (s, Ar-*C*), 125.69 (s, Ar-CH), 124.88 (s, Ar-CH), 123.76 (s, Ar-CH), 123.58 (s, Ar-CH), 25.55 (s, *C*H(CH$_3$)$_2$), 23.44 (s, *C*H(CH$_3$)$_2$), 20.58 (vt, CH(*C*H$_3$)$_2$), 20.10 (s, CH(*C*H$_3$)$_2$), 19.58 (s, CH(*C*H$_3$)$_2$), 18.45 (vt, CH(*C*H$_3$)$_2$). Elemental analysis: Calcd (%): C, 42.40; H, 4.92. Found: C, 42.09; H, 4.68.

Synthesis of $\mathbf{4}_{\mathbf{OTf}}$. To a solution of $\mathbf{1}_{\mathbf{OTf}}$ (100 mg, 0.165 mmol) in 1 mL of THF was added 2.05 equiv of ONMe$_3$ (26 mg, 0.340 mmol) and allowed to stand until homogeneous. *n*-Pentane was introduced to the solution via vapor diffusion overnight to yield analytically pure red needles of $\mathbf{4}_{\mathbf{OTf}}$. Yield: 60 mg (51%, 0.083 mmol). ^{31}P NMR (243 MHz, THF-d_8) δ 72.76, 63.92. ^{1}H NMR (600 MHz, THF-d_8) δ 7.56−7.46 (m, 2H, Aryl-*H*), 7.38−7.33 (m, 1H, Aryl-*H*), 7.30 (t, J = 7.7 Hz, 1H, Aryl-*H*), 7.23−7.19 (m, 1H, Aryl-*H*), 7.14 (t, J = 7.8 Hz, 1H, Aryl-*H*), 7.06 (d, J = 7.8 Hz, 1H, Aryl-*H*), 6.32 (dd, J = 8.1, 3.7 Hz, 1H, Aryl-*H*), 4.13 (s, 1H, Ni−C*H*), 3.30 (d, J = 2.6 Hz, 9H, ON(C*H*$_3$)$_3$), 2.94−2.84 (m, 1H, C*H*(CH$_3$)$_2$), 2.74−2.63 (m, 1H, C*H*(CH$_3$)$_2$), 2.54−2.44 (m, 1H, C*H*(CH$_3$)$_2$), 2.25−2.16 (m, 1H, C*H*(CH$_3$)$_2$), 1.54

DOI: 10.1021/acs.inorgchem.7b02766
Inorg. Chem. XXXX, XXX, XXX−XXX

(dd, J = 16.6, 7.0 Hz, 3H, $CH(CH_3)_2$), 1.49−1.30 (m, 18H, $CH(CH_3)_2$), 1.19 (dd, J = 16.1, 6.9 Hz, 3H, $CH(CH_3)_2$). ^{13}C NMR (151 MHz, THF-d_8) δ 157.84 (d, J = 29.5 Hz, C_{Aryl}), 156.76 (d, J = 5.5 Hz, C_{Aryl}), 135.05 (d, J = 47.2 Hz,, P-$C_{\mathbf{Aryl}}$), 132.08 (d, J = 2.6 Hz, C_{Aryl}), 131.62 (d, J = 11.2 Hz, C_{Aryl}), 130.85, C_{Aryl}, 130.63 (d, J = 2.6 Hz, C_{Aryl}), 129.29 (d, J = 14.6 Hz, C_{Aryl}), 126.63 (d, J = 9.3 Hz, C_{Aryl}), 126.33 (d, J = 6.1 Hz, C_{Aryl}), 122.55 (d, J = 83.9 Hz, O = P-C_{Aryl}), 121.95 (d, J = 12.1 Hz, C_{Aryl}), 59.24 (O−$N(CH_3)_3$), 32.28 (dd, J = 20.4, 6.7 Hz, Ni−CH), 26.29 (d, J = 64.3 Hz, $CH(CH_3)_2$), 24.83 (d, J = 22.6 Hz, $CH(CH_3)_2$), 24.55 (d, J = 2.5 Hz, $CH(CH_3)_2$), 22.50 (d, J = 23.6 Hz, $CH(CH_3)_2$), 18.57 (dd, J = 9.2, 2.8 Hz, $CH(CH_3)_2$), 17.68 (d, J = 3.4 Hz, $CH(CH_3)_2$), 16.39 (d, J = 4.2 Hz, $CH(CH_3)_2$), 15.80 ($CH(CH_3)_2$), 15.43 (dd, J = 21.5, 3.2 Hz, $CH(CH_3)_2$), 14.50 (d, J = 3.4 Hz, $CH(CH_3)_2$). ^{19}F NMR (471 MHz, THF-d_8) δ −78.2. Elemental analysis: Calcd (%): C 49.87; H 6.64; N 2.01. Found: C 49.81; H 6.72; N 2.10.

Synthesis of $\mathbf{5_{OTf}}$. To a solution of $\mathbf{2_{OTf}}$ (10 mg, 0.0165 mmol) in 0.7 mL of THF-d_8 was added ~2 equiv of $ONMe_3$ (3 mg, 0.04 mmol) and allowed to stand for 3 h until homogeneous. Analysis by ^{31}P{^{1}H} NMR spectrometry shows complete conversion of the starting material to one major product affording 1:1 peaks. n-Pentane was introduced to the solution via vapor diffusion overnight to yield red crystalline needles of $\mathbf{5_{OTf}}$. However, because of contamination with $ONMe_3$, no yield was determined and the sample was unsuitable for elemental analysis. ^{31}P NMR (243 MHz, THF-d_8) δ 71.9, 63.7. ^{1}H NMR (600 MHz, THF-d_8) δ 6.86−6.79 (m, 2H, Aryl-H), 6.75 (dd, J = 13.1, 2.8 Hz, 1H, Aryl-H), 6.66 (dd, J = 8.0, 2.4 Hz, 1H, Aryl-H), 6.58 (dd, J = 9.0, 2.7 Hz, 1H, Aryl-H), 6.30 (dd, J = 8.9, 4.5 Hz, 1H, Aryl-H), 3.92 (s, 1H, Ni−CH), 3.29 (s, 9H, $ON(CH_3)_3$), 2.96 (s, 6H, $N(CH_3)_2$), 2.90 (s, 6H, $N(CH_3)_2$), 2.68−2.58 (m, 1H, $CH(CH_3)_2$), 2.44 (dp, J = 9.5, 6.9 Hz, 1H, $CH(CH_3)_2$), 2.18 (dq, J = 13.5, 6.6 Hz, 1H, $CH(CH_3)_2$), 1.55 (dd, J = 16.2, 7.1 Hz, 3H, $CH(CH_3)_2$), 1.46 (dd, J = 15.3, 7.1 Hz, 3H, $CH(CH_3)_2$), 1.42−1.31 (m, 15H, $CH(CH_3)_2$), 1.20 (dd, J = 15.8, 7.0 Hz, 3H, $CH(CH_3)_2$). The fourth multiplet for P−$CH(CH_3)_2$ is unresolved from the singlets for $N(CH_3)_2$. ^{13}C NMR (126 MHz, THF-d_8) δ 148.78 (d, J = 7.2 Hz, C_{Aryl}), 145.35 (d, J = 13.9 Hz, C_{Aryl}), 145.08 (d, J = 29.8 Hz, C_{Aryl}), 143.27 (d, J = 5.4 Hz, C_{Aryl}), 134.65 (d, J = 46.3 Hz, C_{Aryl}), 128.38 (d, J = 16.9 Hz, C_{Aryl}), 127.40 (d, J = 14.5 Hz, C_{Aryl}), 127.07 (d, J = 11.1 Hz, C_{Aryl}), 122.18 (d, J = 83.9 Hz, C_{Aryl}), 115.65 (dd, J = 68.9, 2.6 Hz, C_{Aryl}), 114.29 (d, J = 13.4 Hz, C_{Aryl}), 111.66 (C_{Aryl}), 58.58 ($ON(CH_3)$), 39.16 ($N(CH_2)$), 39.07 ($N(CH_2)$), 29.80 (dd, J = 19.5, 6.7 Hz, Ni−CH), 25.70 (d, J = 64.2 Hz, $CH(CH_3)_2$), 21.90 (d, J = 22.7 Hz, $CH(CH_3)_2$), 18.19 (d, J = 2.7 Hz, $CH(CH_3)_2$), 18.09 (d, J = 4.0 Hz, $CH(CH_3)_2$), 17.20 (d, J = 3.7 Hz, $CH(CH_3)_2$), 16.11 (d, J = 3.7 Hz, $CH(CH_3)_2$), 15.25 ($CH(CH_3)_2$), 15.11 (d, J = 3.5 Hz, $CH(CH_3)_2$), 14.88 (d, J = 2.3 Hz, $CH(CH_3)_2$), 14.12 (d, J = 3.4 Hz, $CH(CH_3)_2$). Two signals for P-$\mathbf{C}(CH_3)_2$ are unresolved from the residual solvent peak. ^{19}F NMR (471 MHz, THF-d_8) δ −80.1.

Synthesis of $\mathbf{6_{SbF_6}}$. To a 25 mL thick-walled glass vessel equipped with a Kontes needle valve were added $\mathbf{3_{SbF_6}}$ (51 mg, 0.058 mmol) and trimethylamine-N-oxide (9 mg, 0.120 mmol). The solids were suspended in 20 mL of toluene and sonicated for 18 h. The mother liquor was decanted from the resulting pink precipitate. The solid was washed with 6 mL of pentane in a 2-mL sintered frit funnel and dried in vacuo to yield a pink solid. Crystals suitable for analysis via single-crystal XRD studies were grown from a concentrated solution in dichloromethane layered with hexanes and placed in a freezer at −30 °C for 3 days. Yield: 31 mg (0.035 mmol, 60%). ^{31}P NMR (203 MHz, acetone-d_6) δ 72.9, 50.9. ^{1}H NMR (500 MHz, acetone-d_6) δ 7.97−7.90 (m, 3H, Ar-H), 7.88 (d, $^3J_{HH}$ = 8.1 Hz, 1H, Ar-H), 7.47−7.40 (m, 3H, Ar-H), 7.37 (t, $^3J_{HH}$ = 7.7 Hz, 1H, Ar-H), 4.41 (s, 1H, Ni−CH), 3.43 (s, 9H, $ON(CH_3)_3$), 3.29 (q, $^3J_{HH}$ = 7.3 Hz, 1H, $CH(CH_3)_2$), 2.87 (dp, $^3J_{HH}$ = 14.1, 7.2 Hz, 1H, $CH(CH_3)_2$), 2.70 (dt, $^3J_{HH}$ = 14.5, 7.2 Hz, 1H, $CH(CH_3)_2$), 2.57 (dp, $^3J_{HH}$ = 13.8, 6.9 Hz, 1H, $CH(CH_3)_2$), 1.65 (dd, $^3J_{HP}$ = $^3J_{HH}$ = 17.2, 7.0 Hz, 3H, $CH(CH_3)_2$), 1.59−1.30 (m, 21H, $CH(CH_3)_2$). ^{13}C NMR (126 MHz, acetone-d_6) δ 172.94 (d, J_{CP} = 8.0 Hz, Ar-C), 168.95 (d, J_{CP} = 39.4 Hz, Ar-C), 147.01 (d, J_{CP} = 8.2 Hz, Ar-C), 140.69 (d, J_{CP} = 15.3 Hz, Ar-C), 138.89 (d, J_{CP} = 13.0 Hz, Ar-C), 137.24 (d, J_{CP} = 2.2 Hz, Ar-C), 131.18 (d, J_{CP} = 42.4 Hz, Ar-C), 129.39 (d, J_{CP} = 90.4 Hz, Ar-C), 126.65 (s, Ar-C), 126.11 (s, Ar-C), 125.87 (d, J_{CP} = 10.9 Hz, Ar-C), 124.82 (d, J_{CP} = 12.4 Hz, Ar-C), 124.26 (s, Ar-C), 123.52 (s, Ar-C), 122.03 (s, Ar-C), 111.74 (d, J_{CP} = 85.6 Hz, Ar-C), 60.41($ONCH_3$), 27.65 (d, J_{CP} = 69.5 Hz, $CH(CH_3)_2$), 26.20 (d, $^1J_{CP}$ = 11.5 Hz, $CH(CH_3)_2$), 25.72 (s, $CH(CH_3)_2$), 25.19 (d, $^1J_{CP}$ = 23.5 Hz, $CH(CH_3)_2$), 24.00 (d, $^2J_{CP}$ = 24.2 Hz, $CH(CH_3)_2$), 21.41 (s, $CH(CH_3)_2$), 20.35 (s, $CH(CH_3)_2$), 19.96−19.71 (m, $CH(CH_3)_2$), 18.90−18.62 (m, $CH(CH_3)_2$), 16.79 (s, $CH(CH_3)_2$), 16.19 (d, $^2J_{CP}$ = 3.1 Hz, $CH(CH_3)_2$), 15.85 (d, $^2J_{CP}$ = 4.1 Hz, $CH(CH_3)_2$), 15.39 (d, $^2J_{CP}$ = 3.5 Hz, $CH(CH_3)_2$). HRMS (APCI) Calcd: 585.1109, Found: 585.1211.

Synthesis of $\mathbf{7_{SbF_6}}$. To a solution of $\mathbf{1_{SbF_6}}$ (100 mg, 0.130 mmol) in 4 mL of THF was added 2.05 equiv of $ONPh_2Me$ (55 mg, 0.340 mmol), resulting in an immediate color change to violet. n-Pentane (15 mL) was layered onto the reaction mixture and left to stand at room temperature overnight to yield a purple oil. The oil was dried under high vacuum to yield a purple solid. The solution was taken up in 4 mL THF and the precipitation of the product as an oil using n-pentane was repeated twice, followed by drying under high vacuum to yield an analytically pure sample of $\mathbf{7_{SbF_6}}$. Crystals suitable for analysis by single-crystal XRD studies were grown by layering 1 mL of a 5 mg/mL 1,4-dioxane solution of the title complex with cyclohexane, yielding purple blocks. Yield: 67 mg (65%, 0.084 mmol). ^{31}P NMR (243 MHz, methylene chloride-d_2) δ 81.0, 71.0. ^{1}H NMR (600 MHz, methylene chloride-d_2) δ 7.53−7.41 (m, 3H, Aryl-H), 7.35−7.15 (m, 4H, Aryl-H), 6.28 (dd, J = 8.0, 3.5 Hz, 1H, Aryl-H), 4.37 (s, 1H, Ni−CH), 3.66 (s, 4H, THF O−CH_2), 2.62−2.42 (m, 1H, $CH(CH_3)_2$), 2.25 (m, 3H, $CH(CH_3)_2$), 1.89 (s, 4H, THF O−CH_2−CH_2) 1.72 (dd, J = 16.1, 7.1 Hz, 3H, $CH(CH_3)_2$), 1.67 (dd, J = 15.6, 7.0 Hz, 3H, $CH(CH_3)_2$), 1.29 (dd, J = 16.3, 7.2 Hz, 3H, $CH(CH_3)_2$), 1.22 (dd, J = 15.5, 7.1 Hz, 3H, $CH(CH_3)_2$), 1.17−1.07 (m, 12H, $CH(CH_3)_2$). ^{13}C NMR (151 MHz, methylene chloride-d_2) δ 157.82 (d, J = 5.6 Hz, C_{Aryl}), 148.14 (d, J = 4.4 Hz, C_{Aryl}), 134.34 (d, J = 2.7 Hz, C_{Aryl}), 132.21 (d, J = 11.8 Hz, C_{Aryl}), 132.13 (d, J = 2.5 Hz, C_{Aryl}), 130.16 (d, J = 12.5 Hz, C_{Aryl}), 129.93 (d, J = 9.7 Hz, C_{Aryl}), 126.41 (d, J = 12.1 Hz, C_{Aryl}), 125.37 (d, J = 9.3 Hz, C_{Aryl}), 123.34 (d, J = 84.6 Hz, O−P C_{Aryl}), 122.30 (d, J = 12.1 Hz, C_{Aryl}), 121.06 (d, J = 83.0 Hz, O−P C_{Aryl}), 25.94 (d, J = 65.4 Hz, $CH(CH_3)_2$), 25.07 (d, J = 23.7 Hz, $CH(CH_3)_2$), 25.05 (d, J = 66.1 Hz, $CH(CH_3)_2$), 24.63 (d, J = 26.0 Hz, $CH(CH_3)_2$), 15.88 (($CH(CH_3)_2$), 15.72 (d, J = 2.7 Hz, ($CH(CH_3)_2$), 15.42 (d, J = 2.6 Hz, ($CH(CH_3)_2$), 15.38 (d, J = 4.1 Hz, ($CH(CH_3)_2$), 15.24 (d, J = 3.7 Hz, ($CH(CH_3)_2$), 15.11 (d, J = 3.2 Hz, ($CH(CH_3)_2$), 14.47 (d, J = 2.9 Hz, ($CH(CH_3)_2$), 13.98 (d, J = 3.4 Hz, ($CH(CH_3)_2$), 13.37−13.14 (m, Ni-C). Peaks for bound THF are not observed. HRMS (APCI) Calcd: 489.1622, Found: 489.1625. Elemental analysis: Calcd (%): C 43.70; H 5.56. Found: C 43.80; H 5.47.

■ RESULTS AND DISCUSSION

The ligand attachment procedure used to make the bromo derivative of $\mathbf{L_1}$, $\mathbf{1_{Br}}$,[41,43] (Scheme 2) was employed to prepare the new compounds $\mathbf{2}$−$\mathbf{3_{Br}}$. In order to explore oxygen atom transfer to Ni(II) complexes of ligands $\mathbf{L_{1-3}}$, starting materials with more weakly coordinating anions were required. Thus, the bromo complexes were converted to the triflate and hexafluoroantimonate synthons $\mathbf{1_{OTf}}$, $\mathbf{2_{OTf}}$, $\mathbf{1_{SbF_6}}$, and $\mathbf{3_{SbF_6}}$, as depicted in Scheme 2. Bromide abstraction from $\mathbf{1_{Br}}$ with silver salts AgX (X = OTf, SbF_6), which is a strategy previously shown to be effective in related POCOPNi(II) complexes,[45] cleanly effected ion exchange, yielding AgBr as a precipitate and $\mathbf{1_{OTf}}$ or $\mathbf{1_{SbF_6}}$, respectively. In both cases, a color change from dark orange to red was noted and a small upfield shift in the ^{31}P{^{1}H} NMR spectral resonance (44.5 to 44.1 (X = OTf) or 43.1 (X = SbF_6) ppm, respectively) was observed. Structural elucidation by single-crystal XRD experiments revealed that, in the case of $\mathbf{1_{OTf}}$, the counterion is bound directly to the Ni(II)

Scheme 2

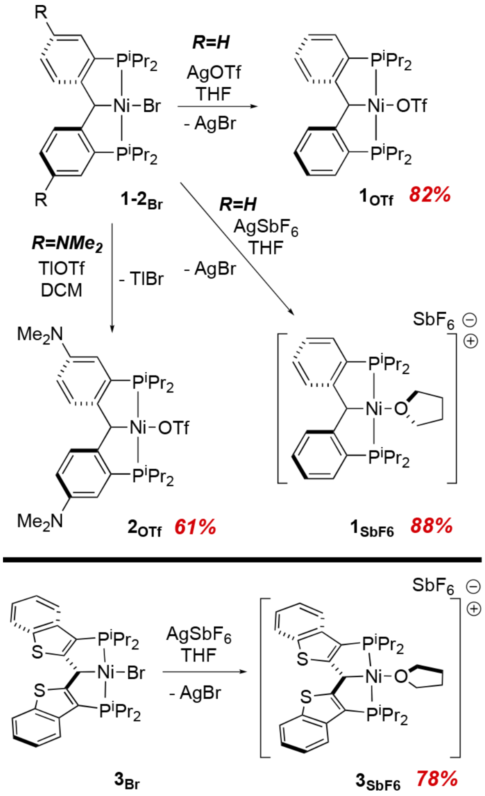

center in the solid state, whereas in $\mathbf{1_{SbF_6}}$, the counterion is displaced from the metal center by a THF solvent molecule. The synthesis of $\mathbf{3_{SbF_6}}$ was successfully carried out from $\mathbf{3_{Br}}$, using the same protocol as $\mathbf{1_{SbF_6}}$. This reaction was similarly accompanied by a color change from red-brown to red-purple and an upfield shift of the resonance in the $^{31}P\{^1H\}$ NMR signal from 40.7 ppm to 37.2 ppm. Both $\mathbf{1_{SbF_6}}$ and $\mathbf{3_{SbF_6}}$ feature broad signals in their NMR spectra, likely due to exchange of the bound and free THF molecules on the NMR time scale.

In contrast, attempted abstraction of bromide from the NMe_2 substituted $\mathbf{2_{Br}}$ with silver salts resulted in an immediate color change from orange to dark blue, the formation of silver metal, and the complete loss of a $^{31}P\{^1H\}$ NMR spectral signature, suggesting a paramagnetic product. This is perhaps unsurprising, given the known propensity of silver salts to oxidize PNPNi(II) complexes,[29,46] and likely involves oxidation of the pendant NMe_2 group on the ligand. Attempted bromide abstractions using KOTf and NaOTf were unsuccessful but ion exchange was accomplished cleanly by using TlOTf (Scheme 2), resulting in a color change from orange to red, similar to $\mathbf{1_{OTf}}$, and an upfield shift in the $^{31}P\{^1H\}$ NMR spectra (from 45.4 ppm to 43.1 ppm).

Structurally, $\mathbf{1_{OTf}}$ and $\mathbf{2_{OTf}}$ are closely related (see Figure 1), with comparable Ni−P bond lengths (2.209 Å vs 2.202 Å avg.), Ni−C bond lengths (1.963(3) Å and 1.975(6) Å), and Ni−O bond lengths (2.003(3) Å vs 2.003(4) Å). The angles around the nickel center are different, with more distortion from idealized square planar geometry in $\mathbf{1_{OTf}}$ than $\mathbf{2_{OTf}}$ ($\tau_4 = 0.22$ vs 0.15)[47] and more torsion between the ligand arene rings (55.67° vs 43.68°; throughout this discussion, these torsion values refer to the angle between the planes defined by the linking aryl rings of the pincer ligand arms). The precise origin of the increased distortion in $\mathbf{1_{OTf}}$ is unknown.

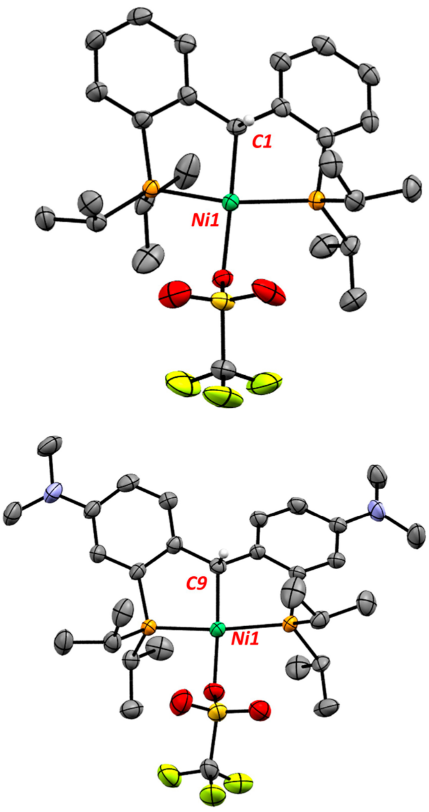

Figure 1. Molecular structure of $\mathbf{1_{OTf}}$ (top) and $\mathbf{2_{OTf}}$ (bottom). Thermal ellipsoids shown to 50% probability. Most hydrogen atoms are omitted for the sake of clarity. Select distances for $\mathbf{1_{OTf}}$: Ni1−C1, 1.963(3) Å; P1−Ni1, 2.189(1) Å; Ni1−P2, 2.230(1) Å; Ni1−O1, 2.003(3) Å. Select angles for $\mathbf{1_{OTf}}$: ∠O1−Ni1−P2, 97.43(8)°; ∠O1−Ni1−C1, 170.6(1)°; ∠O1−Ni1−P1, 95.73(8)°; ∠P2−Ni1−P1, 158.44(4)°; $C_{aryl}-C_{aryl}$ torsion angle, 55.67°. Select distances for $\mathbf{2_{OTf}}$: Ni1−C9, 1.975(6) Å; P1−Ni1, 2.230(2) Å; Ni1−P2, 2.174(1) Å; Ni1−O1, 2.003(4) Å. Select angles for $\mathbf{2_{OTf}}$: ∠O1−Ni1−P2, 92.5(1)°; ∠O1−Ni1−C1, 172.5(2)°; ∠O1−Ni1−P1, 97.0(1)°; ∠P2−Ni1−P1, 166.3(6)°; $C_{aryl}-C_{aryl}$ torsion angle, 43.68°.

Oxygen atom transfer to compounds $\mathbf{1-2_{OTf}}$ was explored by reaction of these contact ion pairs with an excess of commercially available $ONMe_3$ in THF (Scheme 3). The reaction proceeded smoothly, resulting in a products characterized by two singlets integrating to 1:1 in the $^{31}P\{^1H\}$ NMR spectra. Furthermore, the ^1H NMR spectra demonstrate a decrease in symmetry characteristic of a change from a C_s to a C_1 symmetric compound and generation of 1 equiv of NMe_3 was confirmed by the presence of a characteristic singlet at 2.13 ppm integrating to 9 protons. The reactions only required 2 equiv of $ONMe_3$ to reach completion. The reaction of $\mathbf{1_{OTf}}$ with $ONMe_3$ was explored in a variety of solvents ($(CD_3)_2CO$, CD_2Cl_2, C_6D_6, and THF-d_8), and, in all cases, the same product was formed within 1 h, with a qualitative solvent rate dependence of $(CD_3)_2CO > CD_2Cl_2 >$ THF-d_8 > C_6D_6. The observed rate dependence may be due to the relatively low solubility of $ONMe_3$ in C_6D_6 and THF-d_8, and/or the increased rate of reaction in more polar solvents. Vapor diffusion of *n*-pentane into the reaction mixture allowed for isolation of a red crystalline solid. Subsequent XRD studies revealed the product to be the result of oxygen-atom transfer to

Scheme 3

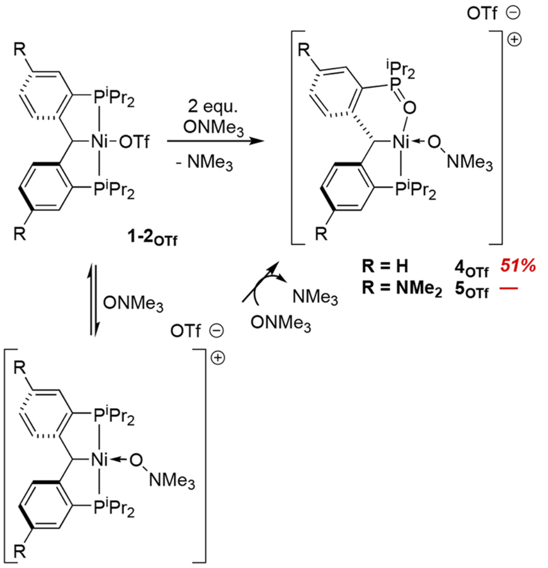

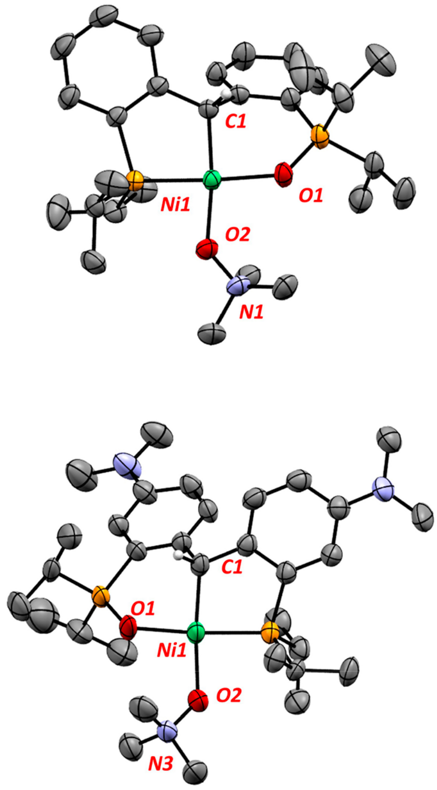

Figure 2. Molecular structure of 4_{OTf} (top) and 5_{OTf} (bottom). Thermal ellipsoids shown to 50% probability. Most hydrogen atoms and counteranions omitted for clarity. Select distances for 4_{OTf}: Ni1–O2, 1.944(2) Å; O2–N1, 1.405(3) Å; Ni1–O1, 1.958(2) Å; P1–Ni1, 2.1195(6) Å; Ni1–C1, 1.948(2) Å; O1–P2, 1.521(2) Å. Select angles for 4_{OTf}: ∠O2–Ni1–C1, 171.53(9)°; ∠O2–Ni1–P1, 87.12(6)°; ∠O2–Ni1–O1, 96.31(8)°; ∠O1–Ni1–P1, 176.48(6)°; ∠Ni1–O1–P2, 130.8(1)°; C_{aryl}–C_{aryl} torsion angle, 66.07°. Select distances for 5_{OTf}: Ni1–C1, 1.945(5) Å; Ni1–P2, 2.114(2) Å; Ni1–O1, 1.938(4) Å; Ni1–O2, 1.950(4) Å. Select angles for 5_{OTf}: ∠O2–Ni1–C1, 173.4(2)°; ∠O1–Ni1–P2, 175.2(1)°; ∠O2–Ni1–O1, 96.2(2)°; ∠O2–Ni1–P2, 88.3(1)°; ∠C1–Ni1–O1, 89.2(2)°; ∠C1–Ni1–P2, 86.4(2)°; C_{aryl}-C_{aryl} torsion angle, 65.63°.

the one of the phosphorus arms of the ligand, resulting in a new PCO ligand system, and displacement of the triflate ion by a second equivalent of ONMe$_3$ to yield 4_{OTf} (see Scheme 3, as well as Figure 2). This asymmetric PCO ligand is unusual, with few examples of similar PCO ligands in the literature.[48,49] However, unlike literature examples, no hemilability of the oxygen arm is observed in 4_{OTf}. Performing the reaction with 1 equiv of ONMe$_3$ in THF results in a 50:50 mix of 4_{OTf} and starting material, and refluxing the reaction mixture does not force the oxidation to completion, indicating that ONMe$_3$ does not undergo exchange between the product and the starting material. At early reaction times, an intermediate was observable by $^{31}P\{^1H\}$ NMR spectroscopy (transient signal at 34.7 ppm) that we hypothesize is due to coordination of ONMe$_3$ to the nickel center, forming an ion separated adduct of $1{-}2_{OTf}$, as shown in Scheme 3. When the reactions were carried out at lower temperatures, this species persisted for lengthier periods, but no other intermediates were ever observed.

That direct coordination of the *N*-oxide to the metal center is required in order to generate product that is supported by the observation that, when compound 1_{Br} was reacted with excess ONMe$_3$ in THF-d_8, the conversion to a new product with $^{31}P\{^1H\}$ resonances at 68.7 and 68.0 ppm was significantly slower than the reaction with 1_{OTf}, with <15% conversion observed after 24 h. Presumably, the much more coordinating Br$^-$ anion slows the rate of the reaction. In a second control experiment, the ability of ONMe$_3$ to oxidize the ligand in the absence of the metal center was probed by the reaction of ONMe$_3$ with the free ligand L_1 in THF-d_8. Again, while the reaction proceeded, its rate was very slow, with free L_1 still present in the sample after 4 days. These results, in addition to the observation of the intermediate postulated in Scheme 3, suggest that the metal must be intimately involved in mediating the oxidation of the ligand by the ONMe$_3$.

To investigate the importance of ligand donor properties on the reaction, the oxidation of 2_{OTf} incorporating the more electron-rich L_2[40] with ONMe$_3$ was effected (Scheme 3). This reaction proceeded in a similar fashion as the oxidation of 1_{OTf}, yielding 5_{OTf} as the major product by $^{31}P\{^1H\}$ NMR spectroscopy, although the rate was slower, with full conversion requiring 3 h in THF, as opposed to 1 h. Monitoring the reaction via $^{31}P\{^1H\}$ NMR spectroscopy reveals a rapid buildup of the ion-separated intermediate adduct (signal at 34.7 ppm), followed by relatively slow O atom transfer to yield the unsymmetrical product 5_{OTf} characterized by two singlets at 71.9 and 63.7 ppm integrating to 1:1 (Figure S1 in the Supporting Information). This decrease in rate is unexpected for a metal-centered oxidation, because the relatively more electron-rich metal center should be more prone to oxidation. Explanations for the decrease in rate include higher lability of the coordinated ONMe$_3$ in the intermediate for the more electron-rich system, or an increase in Ni–P bond strength in 2_{OTf} with the more electron-rich pincer ligand.

The structures of 4_{OTf} and 5_{OTf} are given in Figure 2 and exhibit similar features. In both cases, the nickel center adopts an almost idealized square planar geometry (τ_4 = 0.08 and 0.09),[47] with an increase in torsion between the arenes in the ligand backbone, when compared to the starting complexes (65.63° vs 56.57° and 66.07° vs 43.68°). The bound molecule of ONMe$_3$ in both cases shows little signs of activation in the solid state; the oxygen atom does not appear to be inserting into the remaining Ni–P bond, with O–Ni–P angles of

Scheme 4

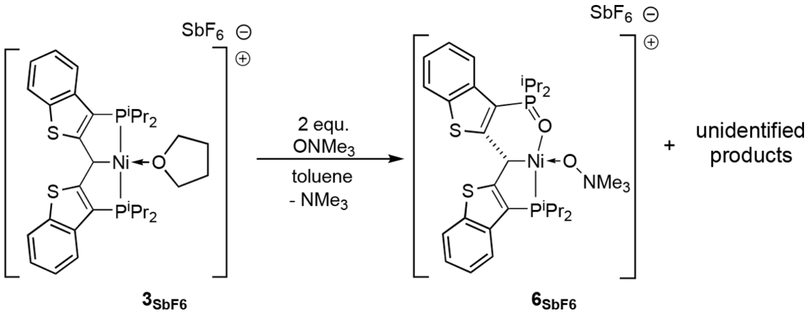

88.3(1)° and 87.12(6)°, nor does there appear to be any lengthening of the O−N bond, with lengths of 1.395(5) and 1.405(3) Å, which are comparable to the literature values of 1.388(5) and 1.404 Å, respectively, for free $ONMe_3$.[50,51]

In order to discourage O atom insertion into the Ni−P bond of the complex, the more-rigid $\mathbf{L_3}$ ligand was enlisted. The use of a five-membered benzothiophene linking group in this system relieves the steric interaction found between the phenyl linkers of $\mathbf{L_1}$ and $\mathbf{L_2}$, creating an overall more planar ligand that would increase this steric interaction upon insertion of an oxygen atom into the N−P bond. Thus, when compared to $\mathbf{1_{SbF_6}}$, $\mathbf{3_{SbF_6}}$ features significantly less torsion between the arene rings of the ligand framework (11.24° vs 51.25°), although the ligand framework still adopts a distorted square planar geometry (τ_4 = 0.19).[47] In the reaction of $\mathbf{3_{SbF_6}}$ with $ONMe_3$ in THF (Scheme 4), similar to both $\mathbf{1_{OTf}}$ and $\mathbf{2_{OTf}}$, formation of an intermediate was signified by the emergence of a signal in the $^{31}P\{^1H\}$ NMR spectra at 30.1 ppm, followed by slow conversion to an asymmetric product characterized by two downfield singlets at 72.5 and 51.1 ppm. However, for $\mathbf{3_{SbF_6}}$, the reaction proceeds far slower than the oxidation of $\mathbf{1_{OTf}}$, with starting material still present after 18 h. Attempts to force the reaction to completion by extending the reaction time or by heating the reaction mixture (up to reflux) leads to the increased formation of unidentified side products. Isolation of the primary product $\mathbf{6_{SbF_6}}$ was accomplished by performing the reaction in toluene and recrystallization of the resultant insoluble residue from methylene chloride/hexanes mixtures. Single-crystal XRD studies revealed the product $\mathbf{6_{SbF_6}}$ to again be the result of oxidation of a ligand phosphine arm (Figure 3). While the starting material $\mathbf{3_{SbF_6}}$ features one of the smallest torsion angles between ligand aromatic linkers, the PCO ligand in $\mathbf{6_{SbF_6}}$ features a much larger torsion angle of 71.19°, suggesting that O atom insertion does indeed engender strong steric interaction between the linker groups of the PCO ligand. The relatively slow rate of this oxidation may be related to this large change in torsion between the ground state and the transition state and/or the lower overall donor properties of $\mathbf{L_3}$.[40]

Since the reaction of $\mathbf{1_{OTf}}$ with the trimethylamine oxide was the most facile, further experiments focused on this parent ligand system ($\mathbf{L_1}$). It was hypothesized that the adduct $\mathbf{4_{OTf}}$ might be induced to transfer a further oxygen atom, but all attempts at further oxidation by release of an oxygen atom from the bound $ONMe_3$ moiety met with failure. Refluxing the sample in either THF or toluene led to slow decomposition over several days and irradiation of the sample with 254 nm light in THF also led to decomposition. Therefore, we turned to other O atom transfer agents. The reagents pyridine *N*-oxide, 2,4,6-trimethylbenzonitrile-*N*-oxide and N_2O were ineffective and did not react with $\mathbf{1_{OTf}}$ in solution, even after 24 h. Motivated by computational reports suggesting that the substitution of methyl groups with phenyl groups in amine-*N*-oxides leads to an increase in thermodynamic oxygen atom donor strength,[50] as well as experimental evidence for an increase in the rate of oxygen transfer of aryl amine *N*-oxides relative to alkyl amine oxides in decarbonylation reactions, despite reduced basicity,[52] the compound $ONMePh_2$ was synthesized via oxidation of the amine with *m*-CPBA.[53] Indeed, reaction of 2 equiv of $ONMePh_2$ with $\mathbf{1_{SbF_6}}$ in THF resulted in an immediate color change from red-orange to bright purple and a new unsymmetrical product was evidenced in both the $^{31}P\{^1H\}$ and ^1H NMR spectra. Signals at 81.0 and 71.0 ppm in the $^{31}P\{^1H\}$ NMR spectrum and a complex ^1H NMR spectrum both suggested C_1 symmetry for the product and furthermore, the ^1H NMR spectrum showed the consumption of both equivalents of $ONMePh_2$ and the formation of 2 equiv of free amine. The compound was isolated as a microcrystalline purple solid. Analysis of the reaction mixture via high-resolution mass spectrometry revealed a mass (M = 489.1625 amu) that was consistent with two oxygen transfers to the nickel-ligand core. On the face of it, these data initially supported the formation of a nickel oxo species. Repeated attempts to garner crystals suitable for X-ray crystallography were plagued by poorly diffracting samples, but crystals obtained from a solution containing a small amount of dioxane did allow for

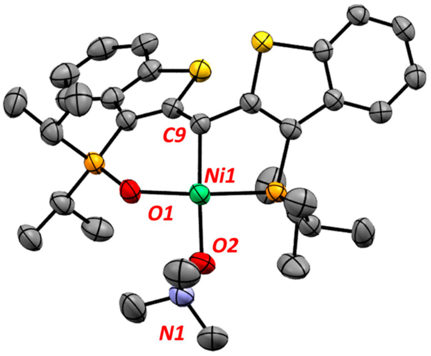

Figure 3. Molecular structure of $\mathbf{6_{SbF_6}}$. Thermal ellipsoids shown to 50% probability. Hydrogen atoms and counteranions omitted for the sake of clarity. Select distances: O1−Ni1, 1.953(4) Å; O2−Ni1, 1.933(3) Å; O2−N1, 1.425(5) Å; P2−Ni1, 2.147(2) Å; Ni1−C9, 1.956(4) Å. Select angles: ∠O2−Ni1−C9, 176.3(2)°; ∠P2−Ni1−O1, 176.1(1)°; ∠O1−Ni1−O2, 94.8(2)°; ∠P2−Ni1−O2, 89.1(1)°; ∠P2−Ni1−C9, 88.0(1)°; ∠O1−Ni1−C9, 88.0(2)°; $C_{aryl}-C_{aryl}$ torsion angle, 71.19°.

DOI: 10.1021/acs.inorgchem.7b02766
Inorg. Chem. XXXX, XXX, XXX−XXX

unambiguous determination of the connectivity within the molecule, showing it to contain the unusual OCO ligand, in which both arms of the pincer ligand **L_1** have been oxidized (see Figure S12 in the Supporting Information). Thus, despite the C_1 symmetry indicated by the NMR spectra of the compound, the isolated product is assigned as the THF adduct **7_{SbF_6}** depicted in Scheme 5, rather than a high-valency nickel oxo species.

Scheme 5

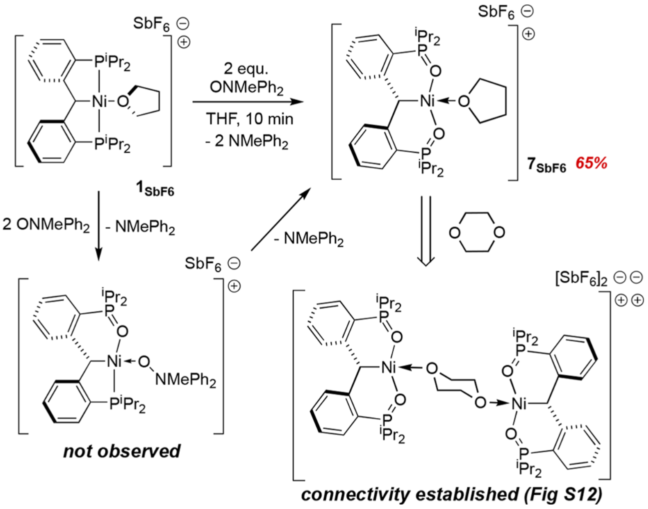

While OCO pincer ligands have been employed in the main group and early-transition-metal complexes,[54−57] group 10 examples are rather rare.[58,59] Compound **7_{SbF_6}** is thermally stable, with no decomposition observed in refluxing THF after 4 h, although it has limited chemical stability, decomposing with the addition of a variety of strong and weak donors, such as PMe_3, $ONMe_3$, pyridine, 4,4′-bipyridine, water, or acetone, although it does not decompose in the presence of PPh_3, even at elevated temperatures. As mentioned above, based on nuclearmagnetic resonance (NMR) spectroscopy, the compound has C_1 symmetry, which is counterintuitive for a product in which both arms of the phosphine are converted to phosphine oxides. However, the expansion of both these chelate rings greatly increases the barrier to exchange of the diastereotopic P environments in **7_{SbF_6}**, because of the steric interaction between the aryl linker rings as the linker arms "flip" conformation. The two phosphines are thus not in exchange on the NMR time scale, and high-temperature NMR spectroscopy reveals that coalescence does not occur up to 65°C in THF.

While the ultimate products of single and double oxygen atom transfer to the Ni(II) cations used here are the result of ligand oxidation, the question remains as to whether or not nickel oxo compounds are involved as intermediates on the reaction path of cations **$1-3_X$** with amine-*N*-oxide reagents. Two possible mechanisms for the oxidation of complex **1_{OTf}** by ONR_3 are shown in Scheme 6. The experimental evidence described above suggests that the first step involves displacement of either a weakly coordinating anion or a coordinated THF molecule by the amine-*N*-oxide to give the transient adducts observed spectroscopically. From this ONR_3 ligated species, transfer of an O atom to the metal with loss of NR_3 (path A, Scheme 6) would yield a transient nickel(IV) oxo complex, which would proceed rapidly to the observed products. In path B, insertion of the O atom proceeds directly via the transition state depicted without the involvement of a nickel oxo species. This question was probed both experimentally via trapping experiments and using DFT computational methods.

Scheme 6

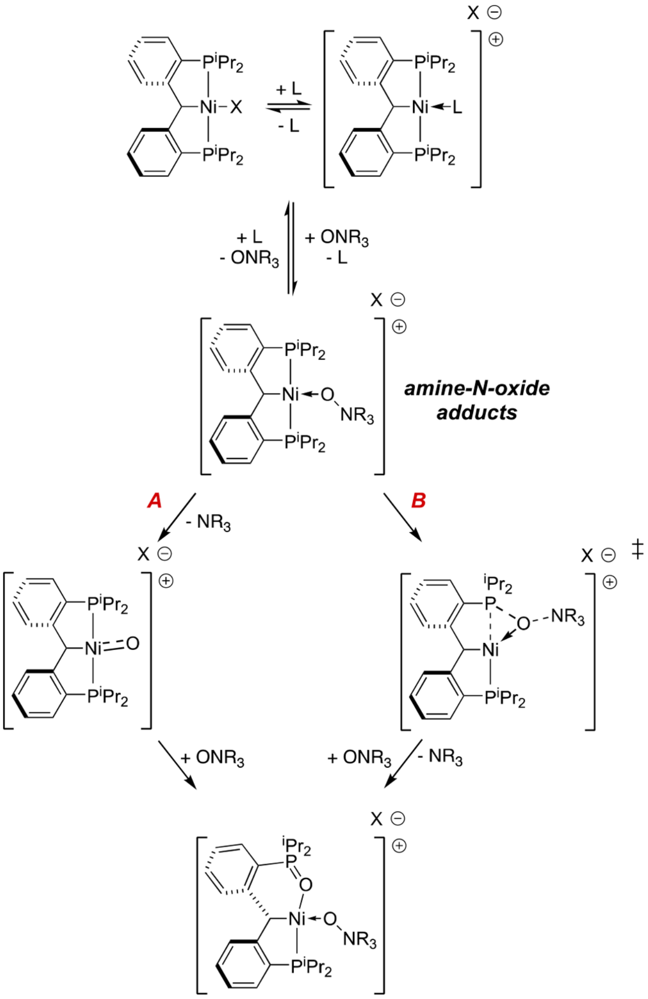

The reaction of **1_{OTf}** with $ONMe_3$ in the presence of 50 equiv of 1,4-cyclohexadiene in THF proceeded cleanly to **4_{OTf}** with no observable formation of either water or benzene.[36] Furthermore, attempted trapping with phosphines[24,35] in THF proceeded with no oxidation, in the case of PPh_3, whereas PMe_3 formed a strong complex with **1_{OTf}**, preventing formation of the necessary adduct with $ONMe_3$. Attempted interception of Ni=O with KH[24] in THF yielded only known compound **L_1**NiH[41] and **4_{OTf}** as products, with no detection of known compound **L_1**NiOH.[41] The addition of excess $Sc(OTf)_3$ or $B(C_6F_5)$, potential Lewis acid trapping agents for a Ni oxo intermediate,[34,60] to the reaction mixture in THF led to no consumption of the **1_{OTf}** starting material, presumably due to sequestering of ONR_3. Finally, freeze-quenched reactions between **1_{OTf}** and ONR_3 in 2-MeTHF showed no observable EPR signals, suggesting a lack of paramagnetic intermediates that are not observable via $^{31}P\{^1H\}$ NMR spectroscopy. Taken together, along with the observation that the more electron-rich **2_{OTf}** system reacts more slowly with the amine-*N*-oxides, the results of these trapping experiments strongly suggest the lack

DOI: 10.1021/acs.inorgchem.7b02766
Inorg. Chem. XXXX, XXX, XXX−XXX

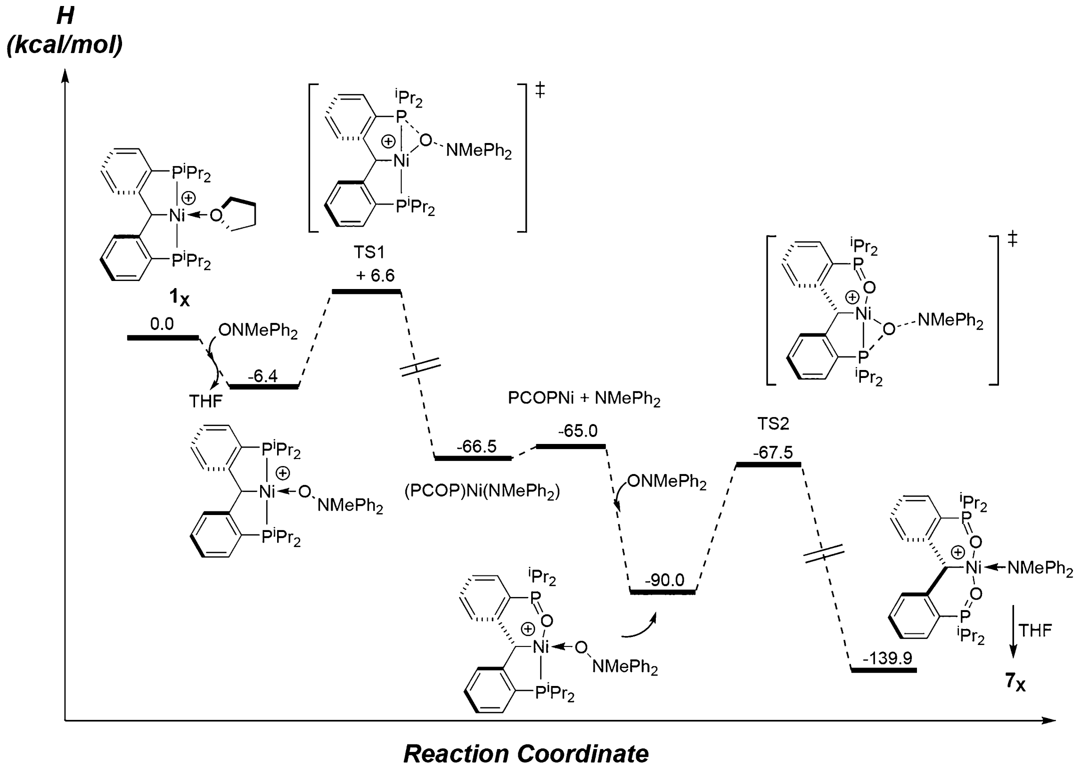

Figure 4. DFT (B3PW91) computed enthalpy reaction profile at 298 K for the oxygen transfer from $\mathrm{ONMePh_2}$ to $[\mathbf{L}_1\mathrm{NiTHF}]^+$.

of a high-valency nickel−oxygen intermediate and favor the direct insertion pathway B in Scheme 6.

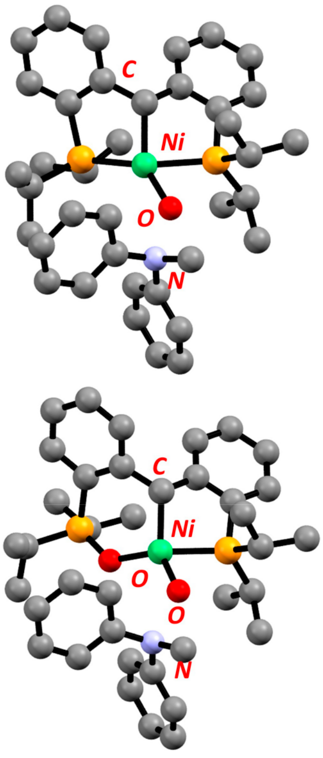

Figure 5. DFT (B3PW91) optimized geometries of the transition states for the first (TS1, top) and second (TS2, bottom) oxygen transfer reactions.

The reaction of $\mathrm{ONMePh_2}$ with the cationic $[\mathbf{L}_1\mathrm{NiTHF}]^+$ fragment was further studied using density functional theory (DFT) methods and the low-energy reaction coordinate for two sequential oxygen atom transfer events is shown in Figure 4. The first step of the reaction was found to be the barrier-less displacement of THF and coordination of *N*-oxide to metal center; these species likely are in equilibrium, and this is completely consistent with experimental observations. This is followed by a low barrier insertion (13.0 kcal/mol) of the oxygen into the Ni−P bond. The geometry of the transition state for the first oxygen transfer (TS1, Figure 5) exhibits considerable N−O bond lengthening in the *N*-oxide fragment when compared to the optimized adduct geometry (1.852 Å vs 1.389 Å), concurrent with a shortening of the P−O bond distance (2.334 Å vs 2.838 Å) and a decrease in P−Ni−O angle (68.37° vs 82.00°). Notably, there is very little lengthening of the Ni−P bond distance, suggesting that phosphine dissociation is not a prerequisite for insertion and consistent with the low calculated barrier for this insertion. Oxidation of the phosphine is exothermic, relative to the starting material, by −66.5 kcal/mol and is further favored by an additional 23.5 kcal/mol through the binding of a second molecule of $\mathrm{ONMePh_2}$ to give a product analogous to the isolated compounds $\mathbf{4}$−$\mathbf{5}_{\mathbf{OTf}}$ and $\mathbf{6}_{\mathbf{SbF_6}}$. Further oxygen transfer from this species is calculated to have a notably higher barrier of 22.5 kcal/mol, when compared to the first oxidation, but is of a magnitude consistent with the rapid reaction observed under ambient conditions for this second oxygen atom transfer when using $\mathrm{ONMePh_2}$. Similar to TS1, TS2 (Figure 5) features an elongated N−O (1.978 Å vs 1.389 Å) distance, a decrease in O−P (2.386 Å vs 2.910 Å) distance and a decrease in P−Ni−O (73.57° vs 88.08°) angle, relative to the adduct, providing no evidence of a divergent mechanism for the second oxidation. Oxidation of the second phosphine arm is similarly exothermic, although the magnitude of thermodynamic stabilization is 10.2 kcal/mol less. This difference in enthalpy could be explained by the increased ligand strain involved in undergoing a second ring expansion within the pincer ligand framework.

These computations suggest that a Ni(IV) oxo species, such as that shown in Scheme 6, analogous to the Pt(IV) species reported previously,[24] does not lie along the pathway of this reaction. Indeed, while DFT minimization of this species does converge on a local minimum, the ground-state structure is a triplet that is best described as a Ni(III) oxyl complex with significant spin density on the oxo ligand (see Figure S13 in the Supporting Information). Furthermore, it is 54.2 kcal/mol higher in energy than the first PCO insertion product, on an energy surface that is not connected to the reaction coordinate in Figure 4. Thus, the formation of such an intermediate can be ruled out for the first insertion reaction. A similar geometry optimization of a putative Ni oxo species formed from the second oxygen atom transfer en route to 7_X was also carried out and again, this is a triplet ground state Ni oxyl that is much higher in energy (56.8 kcal/mol) than the second PCO insertion product (amine adduct in Figure 4). Therefore, forming such Ni oxo/oxyl species, even transiently in these reactions, seems quite unlikely, based on the totality of the experimental and computational results presented.

■ CONCLUSIONS

The implication and harnessing of highly reactive late-transition-metal oxo or nitrido complexes is of current interest. For the former, oxygen atom transfer agents are often used in an effort to generate such species. Here, we have studied the reactions of cationic Ni(II) complexes supported by three pincer ligands with differing steric and electronic properties. Facile reactions with amine-*N*-oxide reagents were discovered, and the products characterized indicated oxygen atom insertion into one or two of the Ni−P bonds of the pincer ligand framework, depending on the stoichiometry of the reaction and the oxygen atom transferring ability of the ONR_3 reagent. The possibility that nickel oxo complexes are involved as intermediates in these reactions was explored both experimentally and computationally, and these investigations indicate that they are not involved on the reaction path. Direct insertion of the oxygen atom into the Ni−P bond(s) offers a much lower energy path to the products than one that goes through a nickel oxo derived from oxygen atom transfer to the metal. This probably is in part due to the flexibility of the pincer ligand and its ability to undergo ring expansion, not only once but twice. Computations do indicate that the barrier to a second O atom insertion is higher than the first, suggesting that increased rigidification through linking the aryl rings[40,61] of the ligand may be a strategy to employ in raising the barrier to direct O atom insertion into the Ni−P bonds. This may make Ni−O formation competitive with direct insertion and allow for generation and implication of a Ni═O, which computations suggest will be a Ni(III) oxyl species.

■ ASSOCIATED CONTENT

Supporting Information

The Supporting Information is available free of charge on the ACS Publications website at DOI: 10.1021/acs.inorg-chem.7b02766.

Experimental and characterization details for all new compounds, including spectroscopic data and computational details (PDF)

X-ray crystallographic data (Cartesian coordinates) (XYZ)

Accession Codes

CCDC 1582263−1582271 contain the supplementary crystallographic data for this paper. These data can be obtained free of charge via www.ccdc.cam.ac.uk/data_request/cif, or by emailing data_request@ccdc.cam.ac.uk, or by contacting The Cambridge Crystallographic Data Centre, 12 Union Road, Cambridge CB2 1EZ, U.K.; fax: +44 1223 336033.

■ AUTHOR INFORMATION

Corresponding Authors

*E-mail: wpiers@ucalgary.ca (W. E. Piers).
*E-mail: laurent.maron@irsamc.ups-tlse.fr (L. Maron).

ORCID

Warren E. Piers: 0000-0003-2278-1269
Laurent Maron: 0000-0003-2653-8557

Notes

The authors declare no competing financial interest.

■ ACKNOWLEDGMENTS

Funding for this work was provided by NSERC of Canada (Discovery Grant) the Canada Research Chair secretariat (Tier I CRC 2013−2020) to W.E.P. The Alexander von Humboldt Foundation (W.E.P. and L.M.) and the Chinese Academy of Science (L.M.) are acknowledged for financial support. L.M. is member of the Institut Universitaire de France. L.M. and W.P. also acknowledge CNRS for a bilateral grant through the PICS program. CalMip is acknowledged for a generous grant of computing time.

■ REFERENCES

(1) Chen, Z.; Yin, G. The reactivity of the active metal oxo and hydroxo intermediates and their implications in oxidations. *Chem. Soc. Rev.* **2015**, *44*, 1083−1100.

(2) Hohenberger, J.; Ray, K.; Meyer, K. The biology and chemistry of high-valent iron-oxo and iron-nitrido complexes. *Nat. Commun.* **2012**, *3*, 720−733.

(3) Ray, K.; Pfaff, F. F.; Wang, B.; Nam, W. Status of reactive non-heme metal-oxygen intermediates in chemical and enzymatic reactions. *J. Am. Chem. Soc.* **2014**, *136*, 13942−13958.

(4) Ortiz de Montellano, P. R. Hydrocarbon hydroxylation by cytochrome P450 enzymes. *Chem. Rev.* **2010**, *110*, 932−948.

(5) Gunay, A.; Theopold, K. H. C−H bond activations by metal oxo compounds. *Chem. Rev.* **2010**, *110*, 1060−1081.

(6) Krest, C. M.; Onderko, E. L.; Yosca, T. H.; Calixto, J. C.; Karp, R. F.; Livada, J.; Rittle, J.; Green, M. T. Reactive intermediates in cytochrome p450 catalysis. *J. Biol. Chem.* **2013**, *288*, 17074−17081.

(7) Yoshizawa, K. Nonradical mechanism for methane hydroxylation by iron-oxo complexes. *Acc. Chem. Res.* **2006**, *39*, 375−382.

(8) Blakemore, J. D.; Crabtree, R. H.; Brudvig, G. W. Molecular Catalysts for Water Oxidation. *Chem. Rev.* **2015**, *115*, 12974−13005.

(9) Karkas, M. D.; Verho, O.; Johnston, E. V.; Akermark, B. Artificial photosynthesis: Molecular systems for catalytic water oxidation. *Chem. Rev.* **2014**, *114*, 11863−12001.

(10) Nocera, D. G. The artificial leaf. *Acc. Chem. Res.* **2012**, *45*, 767−776.

(11) Piers, W. E. Future Trends in Organometallic Chemistry: Organometallic Approaches to Water Splitting. *Organometallics* **2011**, *30*, 13−16.

(12) Lewis, N. S.; Nocera, D. G. Powering the planet: Chemical challenges in solar energy utilization. *Proc. Natl. Acad. Sci. U. S. A.* **2006**, *103*, 15729−15735.

(13) Dempsey, J. L.; Esswein, A. J.; Manke, D. R.; Rosenthal, J.; Soper, J. D.; Nocera, D. G. Molecular chemistry of consequence to renewable energy. *Inorg. Chem.* **2005**, *44*, 6879−6892.

(14) Yagi, M.; Kaneko, M. Molecular catalysts for water oxidation. *Chem. Rev.* **2001**, *101*, 21−35.

(15) Alstrum-Acevedo, J. H.; Brennaman, M. K.; Meyer, T. J. Chemical approaches to artificial photosynthesis. 2. *Inorg. Chem.* **2005**, *44*, 6802−6827.

(16) Ray, K.; Heims, F.; Pfaff, F. F. Terminal Oxo and Imido Transition-Metal Complexes of Groups 9−11. *Eur. J. Inorg. Chem.* **2013**, *2013*, 3784−3807.

(17) Winkler, J. R.; Gray, H. B. In *Molecular Electronic Structures of Transition Metal Complexes I*; Mingos, D. M. P., Day, P., Dahl, J. P., Ed.; Springer: Berlin, Heidelberg, Germany, 2012; pp 17−28.

(18) Betley, T. A.; Wu, Q.; Van Voorhis, T.; Nocera, D. G. Electronic design criteria for O-O bond formation via metal-oxo complexes. *Inorg. Chem.* **2008**, *47*, 1849−1861.

(19) Mayer, J. M. Why Are There No Terminal Oxo Complexes of the Late Transition Metals? or The Importance of Metal−Ligand π Antibonding Interactions. *Comments Inorg. Chem.* **1988**, *8*, 125−135.

(20) Berry, J. F. Terminal Nitrido and Imido Complexes of the Late Transition Metals. *Comments Inorg. Chem.* **2009**, *30*, 28−66.

(21) Efremenko, I.; Poverenov, E.; Martin, J. M.; Milstein, D. DFT study of the structure and reactivity of the terminal Pt(IV)-oxo complex bearing no electron-withdrawing ligands. *J. Am. Chem. Soc.* **2010**, *132*, 14886−14900.

(22) Scheibel, M. G.; Askevold, B.; Heinemann, F. W.; Reijerse, E. J.; de Bruin, B.; Schneider, S. Closed-shell and open-shell square-planar iridium nitrido complexes. *Nat. Chem.* **2012**, *4*, 552−558.

(23) Schoffel, J.; Rogachev, A. Y.; DeBeer George, S.; Burger, P. Isolation and hydrogenation of a complex with a terminal iridium-nitrido bond. *Angew. Chem., Int. Ed.* **2009**, *48*, 4734−4738.

(24) Poverenov, E.; Efremenko, I.; Frenkel, A. I.; Ben-David, Y.; Shimon, L. J. W.; Leitus, G.; Konstantinovski, L.; Martin, J. M. L.; Milstein, D. Evidence for a terminal Pt(IV)-oxo complex exhibiting diverse reactivity. *Nature* **2008**, *455*, 1093−1096.

(25) Tsvetkov, N. P.; Andino, J. G.; Fan, H.; Verat, A. Y.; Caulton, K. G. Reactivity of the terminal oxo species ($(^tBu_2PCH_2SiMe_2)_2N$)RhO. *Dalton Trans.* **2013**, *42*, 6745−6755.

(26) Ingleson, M. J.; Pink, M.; Fan, H.; Caulton, K. G. Redox chemistry of the triplet complex (PNP)Co(I). *J. Am. Chem. Soc.* **2008**, *130*, 4262−4276.

(27) Scheibel, M. G.; Wu, Y.; Stuckl, A. C.; Krause, L.; Carl, E.; Stalke, D.; de Bruin, B.; Schneider, S. Synthesis and reactivity of a transient, terminal nitrido complex of rhodium. *J. Am. Chem. Soc.* **2013**, *135*, 17719−17722.

(28) Schoffel, J.; Susnjar, N.; Nuckel, S.; Sieh, D.; Burger, P. 4d vs. 5d-Reactivity and Fate of Terminal Nitrido Complexes of Rhodium and Iridium. *Eur. J. Inorg. Chem.* **2010**, *2010*, 4911−4915.

(29) Vreeken, V.; Siegler, M. A.; de Bruin, B.; Reek, J. N.; Lutz, M.; van der Vlugt, J. I. C-H Activation of Benzene by a Photoactivated Ni(II)(azide): Formation of a Transient Nickel Nitrido Complex. *Angew. Chem., Int. Ed.* **2015**, *54*, 7055−7059.

(30) Zolnhofer, E. M.; Kass, M.; Khusniyarov, M. M.; Heinemann, F. W.; Maron, L.; van Gastel, M.; Bill, E.; Meyer, K. An intermediate cobalt(IV) nitrido complex and its N-migratory insertion product. *J. Am. Chem. Soc.* **2014**, *136*, 15072−15078.

(31) Vreeken, V.; Baij, L.; de Bruin, B.; Siegler, M. A.; van der Vlugt, J. I. N-Atom transfer via thermal or photolytic activation of a Co-azido complex with a PNP pincer ligand. *Dalton Trans.* **2017**, *46*, 7145−7149.

(32) Hojilla Atienza, C. C.; Bowman, A. C.; Lobkovsky, E.; Chirik, P. J. Photolysis and thermolysis of bis(imino)pyridine cobalt azides: C−H activation from putative cobalt nitrido complexes. *J. Am. Chem. Soc.* **2010**, *132*, 16343−16345.

(33) Adhikari, D.; Basuli, F.; Fan, H.; Huffman, J. C.; Pink, M.; Mindiola, D. J. P = N Bond Formation via Incomplete N-Atom Transfer from a Ferrous Amide Precursor. *Inorg. Chem.* **2008**, *47*, 4439−4441.

(34) Pfaff, F. F.; Kundu, S.; Risch, M.; Pandian, S.; Heims, F.; Pryjomska-Ray, I.; Haack, P.; Metzinger, R.; Bill, E.; Dau, H.; Comba, P.; Ray, K. An oxocobalt(IV) complex stabilized by Lewis acid interactions with scandium(III) ions. *Angew. Chem., Int. Ed.* **2011**, *50*, 1711−1715.

(35) Pfaff, F. F.; Heims, F.; Kundu, S.; Mebs, S.; Ray, K. Spectroscopic capture and reactivity of S = 1/2 nickel(III)-oxygen intermediates in the reaction of a Ni(II)-salt with mCPBA. *Chem. Commun.* **2012**, *48*, 3730−3732.

(36) Corona, T.; Pfaff, F. F.; Acuna-Pares, F.; Draksharapu, A.; Whiteoak, C. J.; Martin-Diaconescu, V.; Lloret-Fillol, J.; Browne, W. R.; Ray, K.; Company, A. Reactivity of a Nickel(II) Bis(amidate) Complex with meta-Chloroperbenzoic Acid: Formation of a Potent Oxidizing Species. *Chem.—Eur. J.* **2015**, *21*, 15029−15038.

(37) Gelman, D.; Musa, S. Coordination Versatility of sp^3-Hybridized Pincer Ligands toward Ligand−Metal Cooperative Catalysis. *ACS Catal.* **2012**, *2*, 2456−2466.

(38) Gelman, D.; Romm, R. PC(*sp*^{3})P transition metal pincer complexes: Properties and catalytic applications. *Top. Organomet. Chem.* **2013**, *40*, 289−318.

(39) Burford, R. J.; Piers, W. E.; Parvez, M. β-Elimination-Immune PC$_{\text{carbene}}$P Iridium Complexes via Double C−H Activation: Ligand−Metal Cooperation in Hydrogen Activation. *Organometallics* **2012**, *31*, 2949−2952.

(40) Smith, J. D.; Logan, J. R.; Doyle, L. E.; Burford, R. J.; Sugawara, S.; Ohnita, C.; Yamamoto, Y.; Piers, W. E.; Spasyuk, D. M.; Borau-Garcia, J. Cationic mono and dicarbonyl pincer complexes of rhodium and iridium to assess the donor properties of PC$_{\text{carbene}}$P ligands. *Dalton Trans.* **2016**, *45*, 12669−12679.

(41) Gutsulyak, D. V.; Piers, W. E.; Borau-Garcia, J.; Parvez, M. Activation of water, ammonia, and other small molecules by PC$_{\text{carbene}}$P nickel pincer complexes. *J. Am. Chem. Soc.* **2013**, *135*, 11776−11779.

(42) Borau-Garcia, J.; Gutsulyak, D. V.; Burford, R. J.; Piers, W. E. Selective hydration of nitriles to amides catalysed by PCP pincer supported nickel(II) complexes. *Dalton Trans.* **2015**, *44*, 12082−12085.

(43) LaPierre, E. A.; Piers, W. E.; Spasyuk, D. M.; Bi, D. W. Activation of Si−H bonds across the nickel carbene bond in electron rich nickel PC$_{\text{carbene}}$P pincer complexes. *Chem. Commun.* **2016**, *52*, 1361−1364.

(44) Doyle, L. E.; Piers, W. E.; Borau-Garcia, J. Ligand Cooperation in the Formal Hydrogenation of N_2O Using a PC$_{\text{sp2}}$P Iridium Pincer Complex. *J. Am. Chem. Soc.* **2015**, *137*, 2187−2190.

(45) Castonguay, A.; Spasyuk, D. M.; Madern, N.; Beauchamp, A. L.; Zargarian, D. Regioselective Hydroamination of Acrylonitrile Catalyzed by Cationic Pincer Complexes of Nickel(II). *Organometallics* **2009**, *28*, 2134−2141.

(46) DeMott, J. C.; Basuli, F.; Kilgore, U. J.; Foxman, B. M.; Huffman, J. C.; Ozerov, O. V.; Mindiola, D. J. Silver(I) and Thallium(I) Complexes of a PNP Ligand and Their Utility as PNP Transfer Reagents. *Inorg. Chem.* **2007**, *46*, 6271−6276.

(47) Yang, L.; Powell, D. R.; Houser, R. P. Structural variation in copper(I) complexes with pyridylmethylamide ligands: structural analysis with a new four-coordinate geometry index, τ_4. *Dalton Trans.* **2007**, 955−964.

(48) Rybtchinski, B.; Oevers, S.; Montag, M.; Vigalok, A.; Rozenberg, H.; Martin, J. M.; Milstein, D. Comparison of steric and electronic requirements for C−C and C−H bond activation. Chelating vs nonchelating case. *J. Am. Chem. Soc.* **2001**, *123*, 9064−9077.

(49) Fulmer, G. R.; Kaminsky, W.; Kemp, R. A.; Goldberg, K. I. Syntheses and Characterization of Palladium Complexes with a Hemilabile "PCO" Pincer Ligand. *Organometallics* **2011**, *30*, 1627−1636.

(50) Rogachev, A. Y.; Burger, P. Bonding situation and N-O-bond strengths in amine-N-oxides—A combined experimental and theoretical study. *Phys. Chem. Chem. Phys.* **2012**, *14*, 1985−2000.

(51) Caron, A.; Palenik, G. J.; Goldish, E.; Donohue, J. The molecular and crystal structure of trimethylamine oxide, $(CH_3)_3NO$. *Acta Crystallogr.* **1964**, *17*, 102−108.

(52) Shen, J.-K.; Gao, Y.-C.; Shi, Q.-Z.; Basolo, F. Effect of substituents on amine N-oxides on the rates of O-atom transfer to metal carbonyls. *J. Organomet. Chem.* **1991**, *401*, 295−303.

(53) Cymerman Craig, J.; Purushothaman, K. K. Improved preparation of tertiary amine N-oxides. *J. Org. Chem.* **1970**, *35*, 1721−1722.

(54) Agapie, T.; Bercaw, J. E. Cyclometalated Tantalum Diphenolate Pincer Complexes: Intramolecular C−H/M−CH_3 σ-Bond Metathesis May Be Faster than O−H/M−CH3 Protonolysis. *Organometallics* **2007**, *26*, 2957−2959.

(55) Peveling, K.; Henn, M.; Löw, C.; Mehring, M.; Schürmann, M.; Costisella, B.; Jurkschat, K. Mechanistic Studies on the Cyclization of Organosilicon and Organotin Compounds Containing the O,C,O-Coordinating Pincer-Type Ligand {4-t-Bu-2,6-$[P(O)(OR)_2]_2C_6H_2$}- (R = *i*-Pr, Et): Phosphorus (POC)- versus Carbon (POC)-Attack. *Organometallics* **2004**, *23*, 1501−1508.

(56) Mehring, M.; Schurmann, M.; Jurkschat, K. The first rigid O, C,O-Pincer ligand and its application for the synthesis of penta- and hexacoordinate organotin(IV) compounds. *Organometallics* **1998**, *17*, 1227−1236.

(57) Sarkar, S.; Carlson, A. R.; Veige, M. K.; Falkowski, J. M.; Abboud, K. A.; Veige, A. S. Synthesis, characterization, and reactivity of a d^2, Mo(IV) complex supported by a new OCO-trianionic pincer ligand. *J. Am. Chem. Soc.* **2008**, *130*, 1116−1117.

(58) Vicente, J.; Arcas, A.; Blasco, M.-A.; Lozano, J.; Ramírez de Arellano, M. C. Attempts To Prepare Palladium(II) Complexes with the O,C,O Pincer Aryl Ligand $C_6(NO_2)_2$−2,6-$(OMe)_3$−3,4,5. *Organometallics* **1998**, *17*, 5374−5383.

(59) Zhang, Y.; Song, G. Y.; Ma, G. Y.; Zhao, J.; Pan, C. L.; Li, X. W. 1,3-Dinitrone Pincer Complexes of Palladium and Nickel: Synthesis, Structural Characterizations, and Catalysis. *Organometallics* **2009**, *28*, 3233−3238.

(60) Hong, S.; Pfaff, F. F.; Kwon, E.; Wang, Y.; Seo, M. S.; Bill, E.; Ray, K.; Nam, W. Spectroscopic capture and reactivity of a low-spin cobalt(IV)-oxo complex stabilized by binding redox-inactive metal ions. *Angew. Chem., Int. Ed.* **2014**, *53*, 10403−10407.

(61) Yoo, C.; Lee, Y. A T-Shaped Nickel(I) Metalloradical Species. *Angew. Chem., Int. Ed.* **2017**, *56*, 9502−9506.

DOI: 10.1021/acs.inorgchem.7b02766
Inorg. Chem. XXXX, XXX, XXX−XXX